CMS Physics Analysis Summary

Contact: cms-pag-conveners-susy@cern.ch 2016/08/04

Search for SUSY in same-sign dilepton events with 12.9 fb^{-1} of pp collision data at 13 TeV

The CMS Collaboration

Abstract

A search for new physics is performed using events with a pair of isolated same-sign leptons and jets in the final state using the CMS detector at the LHC. Results are based on a sample of proton-proton collisions at a centre-of-mass energy of 13 TeV, corresponding to an integrated luminosity of 12.9 inverse femtobarns. In order to be sensitive to a wide variety of possible signals beyond the standard model, we consider multiple search regions defined by the missing transverse energy, the hadronic transverse energy, the transverse mass, the number of jets and b quark jets, and the transverse momenta of the leptons in the event. No excess above the standard model background expectation is observed and constraints are set on the gluino pair production cross section; model independent limits and selection efficiencies are also provided for additional model testing.

1 Introduction

Searches for new physics in the same-sign (SS) dilepton final state are motivated by the limited number of standard model (SM) processes yielding such a signature and by numerous new physics models producing two same-sign leptons, such as the production of supersymmetric (SUSY) particles, Majorana neutrinos, or same-sign top quark pairs. Among the SUSY processes, gluino pair production can result in same-sign leptons either by generating four top quarks in the decay chain ($\tilde{g} \to t\tilde{t}$, $\tilde{t} \to t\tilde{\chi}_1^0$), or when both gluinos decay to charginos of the same sign ($\tilde{g} \to qq\tilde{\chi}^{\pm}, \tilde{\chi}^{\pm} \to W^{\pm}\tilde{\chi}_1^0$), due to the Majorana nature of the gluino, leading to same-sign W bosons. Alternatively, cascade decays of pair-produced squarks could also lead to the same signature. Rare SM processes, such as the $t\bar{t}$ $t\bar{t}$ production, also lead to SS lepton signature.

Searches for SS dileptons have been carried out previously by the CMS experiment [1] at the CERN LHC, and the results have been published for different analysis strategies with 8 TeV data [2, 3], and with 13 TeV data recorded in 2015 [4]. The 2015 data analysis based on an integrated luminosity of 2.3 fb^{-1} [4] probed gluino masses in the four top quark signature up to about 1.3 TeV. Searches performed by the ATLAS collaboration with 13 TeV data [5] yield similar results.

This physics analysis summary describes a new physics search similar to the one presented in [4]. The search is performed using a data sample ot 13 TeV proton-proton collisions corresponding to an integrated luminosity of 12.9 fb^{-1}, collected with the CMS detector in the first half of 2016. Signal regions definitions have been slightly modified with respect to Ref. [4], benefiting from the larger available data sample and increasing the sensitivity of the search.

2 Event selection and Monte Carlo simulation

The event selection requires the presence of a pair of well-identified and isolated leptons (ee, eμ, or $\mu\mu$). Online, such events are selected by two sets of high-level triggers (HLT). The first set requires two loosely identified and isolated leptons with transverse momentum $p_{\text{T}} > 17$ or 23 GeV for the leading lepton, and $p_{\text{T}} > 12$ (8) GeV for the trailing electron (muon). The second set benefits from lowered p_{T} thresholds for both leptons ($p_{\text{T}} > 8$ GeV), no isolation requirements on the lepton, but demands hadronic activity of $H_{\text{T}}^{\text{HLT}} > 300$ GeV in the event, with $H_{\text{T}}^{\text{HLT}}$ defined as the scalar sum of p_{T} of all jets with $p_{\text{T}} > 30$ GeV and $|\eta| < 3.0$.

Electron candidates are reconstructed by combining tracks in the silicon tracker [6] and clusters of energy deposits in the electromagnetic calorimeter (ECAL). Electron identification is performed using a multivariate discriminant based on the shower shape and track quality variables. The nominal selection criteria are designed to have maximum rejection of electron candidates from QCD multijet production, while maintaining approximately 90% efficiency for electrons from the decay of W/Z bosons; a relaxed selection on the multivariate discriminant is used for the "loose" definition of electron identification. The quality of the electron charge reconstruction is ensured by requiring the consistency between the independent measurements of the charge from the inner tracker and from the ECAL energy deposit. To suppress electrons arising from photon conversions, tracks with missing hits in the innermost layers of the tracking system are rejected.

Muon candidates are reconstructed combining the information from both the silicon tracker and the muon spectrometer in a global fit [7]. The muon identification is performed using the quality of the geometrical matching between the tracker and the muon system measurements.

The quality of the muon charge reconstruction is ensured by an additional criterion on the track quality: $\delta p_{\mathrm{T}}(\mu)/p_{\mathrm{T}}(\mu) < 0.2$.

To ensure that leptons originate from the same collision vertex (defined as the one with the highest sum of p_{T}^2 of associated tracks), the transverse (longitudinal) impact parameter for each lepton must not exceed 0.5 (1) mm, and only leptons with the 3D impact parameter significance below 4 are considered.

Prompt charged leptons produced in decays of W/Z bosons or SUSY particles are usually spatially isolated from the hadronic activity of the event, in constrast to leptons originating from hadron decays or misidentified leptons. In highly Lorentz-boosted systems, as often observed in 13 TeV pp collision data, decay products tend to overlap, making both signatures less discernible. To mitigate that effect, the isolation variable defined in Ref. [4] is considered. This isolation uses three input variables :

- A mini-isolation (I_{mini}) [8] which is computed as a ratio of the scalar sum of transverse momenta of the charged hadrons, neutral hadrons, and photons within a cone of radius $R(p_{\mathrm{T}}^{\ell})$ around the lepton candidate direction at the origin to the transverse momentum of the candidate. The cone radius R depends on lepton p_{T} as

$$R(p_{\mathrm{T}}^{\ell}) = \frac{10\,\mathrm{GeV}}{\min\left[\max\left(p_{\mathrm{T}}^{\ell}, 50\,\mathrm{GeV}\right), 200\,\mathrm{GeV}\right]}. \tag{1}$$

  The varying isolation cone definition takes into account the aperture of b hadron decays as a function of their p_{T}, and reduces the inefficiency from accidental overlap between the lepton and jets in a busy event environment.

- A ratio between the lepton p_{T}^{ℓ} and $p_{\mathrm{T}}^{\mathrm{jet}}$ of a jet containing the lepton:

$$p_{\mathrm{T}}^{\mathrm{ratio}} = \frac{p_{\mathrm{T}}^{\ell}}{p_{\mathrm{T}}^{\mathrm{jet}}}. \tag{2}$$

  The $p_{\mathrm{T}}^{\mathrm{ratio}}$ variable acts as a relative isolation in a larger cone. It improves mini-isolation performance when there are no nearby jets, expecially for low-p_{T} leptons.

- Transverse momentum of the lepton relative to the residual momentum of the closest jet after lepton momentum subtraction:

$$p_{\mathrm{T}}^{\mathrm{rel}} = \frac{|(\vec{p}(\mathrm{jet}) - \vec{p}(\ell)) \times \vec{p}(\ell)|}{|\vec{p}(\mathrm{jet}) - \vec{p}(\ell)|}. \tag{3}$$

  The $p_{\mathrm{T}}^{\mathrm{rel}}$ variable aids in identification of leptons that accidentally overlap with other jets in the event.

For a lepton to be considered as isolated, the following requirement needs to be fulfilled:

$$I_{\mathrm{mini}} < I_1 \wedge (p_{\mathrm{T}}^{\mathrm{ratio}} > I_2 \vee p_{\mathrm{T}}^{\mathrm{rel}} > I_3). \tag{4}$$

The values of the thresholds $I_{\mathrm{i}}, i = 1, 2, 3$, depend on the lepton flavor (see Table 1). Tighter isolation values are used for electrons, as the probability to misidentify one is higher than for muons.

A pair of SS leptons passing the tight identification with invariant mass $m_{\ell\ell} > 8\,\mathrm{GeV}$ must be present for an event to be selected. In order to reduce backgrounds from γ^* or Z boson

Table 1: Multi-isolation working points used in the analysis.

Isolation value	Loose leptons	Tight electrons	Tight muons
I_1	0.4	0.12	0.16
I_2	0	0.80	0.76
I_3(GeV)	0	7.2	7.2

production, events are rejected if there is an additional lepton (tight or loose) that forms an opposite-sign same-flavor pair with $m_{\ell\ell} < 12\,\text{GeV}$ or $76 < m_{\ell\ell} < 106\,\text{GeV}$ with one of the two SS leptons.

Jets and missing transverse energy ($E_{\text{T}}^{\text{miss}}$) are reconstructed with the particle-flow algorithm [9, 10]. For jet clustering, the anti-k_{t} algorithm [11] with a distance parameter of 0.4 is utilized. Jets are required to pass certain quality requirements [12] to remove those consistent with calorimeter noise. After the expected contribution from extra pp collisions is subtracted, jet energies are corrected for residual nonuniformity and nonlinearity of the detector response using a combination of simulation and data [12]. Jets are required to have $p_{\text{T}} > 40\,\text{GeV}$, be within the tracker acceptance $|\eta| < 2.4$, and be separated from loosely identified leptons by a distance of $\Delta R > 0.4$. We require the number of jets in the event (N_{jets}) to be at least 2. Hadronic activity in the event is defined as the scalar sum of selected jet transverse momenta p_{T}'s: $H_{\text{T}} = \sum_{\text{jets}} p_{\text{T}}$. The missing transverse energy $E_{\text{T}}^{\text{miss}}$ is defined as the negative vectorial sum of all particles reconstructed with the particle-flow algorithm. The corrections applied on the jet energies are propagated to the $E_{\text{T}}^{\text{miss}}$ computation.

To identify jets originating from b quarks, a combined secondary vertex algorithm is used. Jets with $p_{\text{T}} > 25\,\text{GeV}$ and $|\eta| < 2.4$ are considered as b-tagged if they pass the medium working point of the algorithm, which provides around 70% efficiency with a mistag rate less than 1% [13–15]. The number of b-tagged jets is referred to as N_{b}. The kinematic selections of reconstructed objects used in this analysis are summarized in Table 2.

Table 2: Kinematic and fiducial requirements on tight (loose) leptons and jets that are used in the analysis.

Object	p_{T} (GeV)	$\lvert\eta\rvert$
Electrons	>15 (7)	<2.5
Muons	>10 (5)	<2.4
Jets	>40	<2.4
b-tagged jets	>25	<2.4

A set of Monte Carlo (MC) simulations are used to estimate the selection efficiencies for various new physics scenarios or rare SM processes and to estimate the SM backgrounds processes with two SS leptons produced by W or Z boson decays (see Section 4).

The SM background samples are produced with the MADGRAPH5 2.2.2 program [16] at leading order (LO) or next-to-leading order (NLO) accuracy in perturbative quantum chromodynamics, with the exception of diboson samples, which are generated with POWHEG v2 [17]. The PYTHIA 8.205 generator [18] with the CUETP8M1 tune [19] is used to simulate parton showering and hadronization. The CMS detector response is modeled with the GEANT4 package [20]. The SUSY signal samples are generated with MADGRAPH5_AMC@NLO program [16] at LO precision, allowing up to two additional partons to be present in the matrix element calculations. The double top pair sample is generated with MADGRAPH5_AMC@NLO program [16]

at NLO precision. Parton showering and hadronization, as well as decays of SUSY particles, are simulated with PYTHIA.The detector simulation is carried out with the CMS fast simulation package [21]. A series of cross checks is performed to ensure that fast simulation results are in agreement with the ones obtained with GEANT4-based detector simulation.

The NNPDF3.0LO [22] parton distribution functions (PDFs) are used for the simulated samples generated at LO, and the NNPDF3.0NLO [22] PDFs for the samples generated at NLO. Simulated events are processed with the same chain of reconstruction programs that is used for data.

3 Search strategy

The analysis strategy presented in this report follows the strategy already used in an earlier search based on 2015 data [4].

Several signal models can produce SS lepton pairs signatures, and those will lead to different event compositions, in numbers of light-flavor jets, b-tagged jets, and W bosons. In addition, the considered SUSY particle mass spectrum will impact the kinematics of final decay products, implying differences in event kinematic variables, such as the p_{T} of the leptons, H_{T}, and $E_{\mathrm{T}}^{\mathrm{miss}}$.

We consider models of gluino pair production decaying via the $\mathrm{t\bar{t}t\bar{t}}\tilde{\chi}_1^0\tilde{\chi}_1^0$ or $\mathrm{q\bar{q}q\bar{q}WW}\tilde{\chi}_1^0\tilde{\chi}_1^0$ channels, where $\tilde{\chi}_1^0$ is the lightest supersymmetric particle (LSP). The Feynman diagrams corresponding to these two models, referred to as T1tttt and T5qqqqWW, are shown in Figure 1. The kinematics of the decay products are determined by the gluino and LSP masses, as well as the chargino mass in the T5qqqqWW model. In addition to these simplified models, we also set limits on the cross section of SS top-quark production, and on that of the rare SM process $\mathrm{t\bar{t}}$ $\mathrm{t\bar{t}}$.

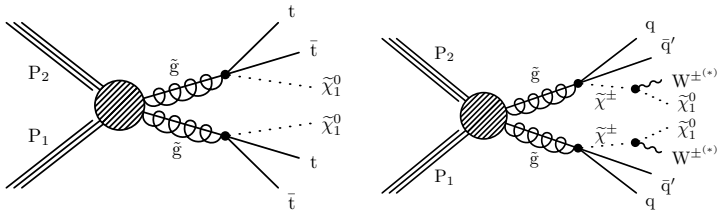

(a) T1tttt (b) T5qqqqWW

Figure 1: Diagrams for SUSY processes possibly yielding two same-sign leptons in the final state.

To be sensitive to a large variety of signal topologies, a number of signal regions are defined using several physics observables, leading to different background composition in these regions.

Three exclusive event selections based on the lepton momenta are defined:

- high-high (HH) selection: two tight leptons with $p_{\mathrm{T}} > 25\,\mathrm{GeV}$;
- high-low (HL) selection: one tight lepton with $p_{\mathrm{T}} > 25$ GeV and one tight lepton with $10 < p_{\mathrm{T}} < 25\,\mathrm{GeV}$; and
- low-low (LL) selection: two tight leptons with $10 < p_{\mathrm{T}} < 25\,\mathrm{GeV}$.

These selections allow to target signals producing high-p_{T} leptons in the HH selection, and compressed-spectrum models inducing soft leptons from off-shell W bosons decays in the HL and LL signal regions. The background composition also differs among the selections, with mostly irreducible SM backgrounds populating the HH region, and leptons not originating

from W or Z boson decays in the HL region. The LL region is characterized by very small background, since all processes with at least one lepton originating from an on-shell vector boson are suppressed by the low-p_{T} requirement.

As the background composition is different for the HH, HL, and LL selections, signal regions are defined separately. The search regions are formed using the N_{jets}, N_{b}, H_{T}, $E_{\mathrm{T}}^{\mathrm{miss}}$, and $M_{\mathrm{T}}^{\mathrm{min}}$ variables, with $M_{\mathrm{T}}^{\mathrm{min}}$ defined as:

$$M_{\mathrm{T}}^{\mathrm{min}} = \min\left(M_{\mathrm{T}}(\ell_1, E_{\mathrm{T}}^{\mathrm{miss}}), M_{\mathrm{T}}(\ell_2, E_{\mathrm{T}}^{\mathrm{miss}})\right),$$

where M_{T} is the transverse mass of the lepton and $E_{\mathrm{T}}^{\mathrm{miss}}$ system. The jet and b-tagged jet multiplicities separate SM backgrounds and signal models, while the separation in H_{T} and $E_{\mathrm{T}}^{\mathrm{miss}}$ bins increase the sensitivity to different SUSY scenarios. The $M_{\mathrm{T}}^{\mathrm{min}}$ variable separates signal-like events from $\mathrm{t\bar{t}}$-like events, as for the latter a cutoff is expected at the W boson mass. Consequently, search regions with $M_{\mathrm{T}}^{\mathrm{min}} > 120\,\mathrm{GeV}$ profit from reduced $\mathrm{t\bar{t}}$ background. The choice of 120 GeV is the result of an optimization study.

With respect to the previous analysis [4], the signal regions HH SR27 and HL SR21 have been merged with their neighboring regions HH SR25 and HL SR19, respectively. This modification is motivated by the very low SM yields predicted in regions HH SR27 and HL SR21. The numbering of the remaining regions has been adjusted accordingly. In addition, for the HH and HL signal regions, each H_{T} and $E_{\mathrm{T}}^{\mathrm{miss}}$ tail region has been split in two, to account for the higher integrated luminosity, by introducing additional tail regions HH SR32, HH SR33, HL SR26, and HL SR27.

The summary of the selection is described in Tables 3–5. All signal regions are exclusive and are further combined statistically to yield the final results (Section 6).

4 Backgrounds

The SM backgrounds for the SS dilepton final state can be divided in three categories:

- **Nonprompt leptons:** Nonprompt leptons originate from heavy-flavor decays, misidentified hadrons, muons from light-meson decays in flight, or electrons from unidentified photon conversions. The dominant contributions are the $\mathrm{t\bar{t}}$ and W + jets processes, depending on the signal regions. For low-$M_{\mathrm{T}}^{\mathrm{min}}$ and low-H_{T} signal regions, the nonprompt leptons represent the largest background contribution.
- **SM processes with SS leptons:** SM processes could yield SS leptons mostly from diboson production and bosons produced in association with a pair of top quarks; the dominant sources are WZ and $\mathrm{t\bar{t}W}$ events for signal regions with zero and one or more b jets, respectively. They are the largest background in the signal regions defined by very tight selection requirements.
- **Charge misidentification:** Events with opposite-sign isolated leptons, where the charge of one electron is misidentified because of severe bremsstrahlung in the tracker material, account for the smallest fraction of background.

The nonprompt lepton background is estimated using the "tight-to-loose" ratio technique based on control samples in data.

First, a control sample (application region) is defined by selecting events with one lepton failing the nominal selection but passing looser isolation requirements. In this sample, events are reweighted by a transfer-factor $T = \epsilon_{\mathrm{TL}}/(1-\epsilon_{\mathrm{TL}})$, where ϵ_{TL} is the probability for a loosely

Table 3: Signal region definitions for the HH lepton selection.

N_b	M_T^{min} (GeV)	E_T^{miss} (GeV)	N_{jets}	$H_T < 300$ GeV	$H_T \in [300, 1125]$ GeV	$H_T \in [1125, 1300]$ GeV	$H_T > 1300$ GeV
0	< 120	$50 - 200$	2-4	SR1	SR2	SR31	SR33
			5+	SR3	SR4		
		$200 - 300$	2-4		SR5		
			5+		SR6		
	> 120	$50 - 200$	2-4		SR7		
			5+		SR8		
		$200 - 300$	2-4				
			5+				
1	< 120	$50 - 200$	2-4	SR9	SR10		
			5+	SR11	SR12		
		$200 - 300$	2-4		SR13		
			5+		SR14		
	> 120	$50 - 200$	2-4		SR15		
			5+		SR16		
		$200 - 300$	2-4				
			5+				
2	< 120	$50 - 200$	2-4	SR17	SR18		
			5+	SR19	SR20		
		$200 - 300$	2-4		SR21		
			5+		SR22		
	> 120	$50 - 200$	2-4		SR23		
			5+		SR24		
		$200 - 300$	2-4				
			5+				
3+	< 120	$50 - 200$	2+	SR25	SR26		
		$200 - 300$			SR27		
	> 120	$50 - 300$	2+	SR28	SR29		
inclusive	inclusive	$300 - 500$	2+	–	SR30		
		> 500			SR32		

Table 4: Signal region definitions for the HL lepton selection.

N_b	M_T^{min} (GeV)	E_T^{miss} (GeV)	N_{jets}	$H_T < 300$ GeV	$H_T \in [300, 1125]$ GeV	$H_T \in [1125, 1300]$ GeV	$H_T > 1300$ GeV
0	< 120	$50 - 200$	2-4	SR1	SR2	SR25	SR27
			5+	SR3	SR4		
		$200 - 300$	2-4		SR5		
			5+		SR6		
1	< 120	$50 - 200$	2-4	SR7	SR8		
			5+	SR9	SR10		
		$200 - 300$	2-4		SR11		
			5+		SR12		
2	< 120	$50 - 200$	2-4	SR13	SR14		
			5+	SR15	SR16		
		$200 - 300$	2-4		SR17		
			5+		SR18		
3+	< 120	$50 - 200$	2+	SR19	SR20		
		$200 - 300$			SR21		
inclusive	> 120	$50 - 300$	2+	SR22	SR23		
inclusive	inclusive	$300 - 500$	2+	–	SR24		
		> 500			SR26		

isolated and identified nonprompt lepton to pass the nominal selection. The probability ϵ_{TL} is measured in a multijet-enriched data set (measurement region), defined by single-lepton events, from which (Drell–Yan and W + jets) processes are suppressed by the M_T and E_T^{miss} requirements and their residual contamination subtracted. The probability ϵ_{TL} is parametrized as function of the isolation applied at the trigger level, and as function of the lepton flavor, η, and p_T^{corr}, defined as the p_T plus the energy in the isolation cone exceeding the isolation

Table 5: Signal region definitions for the LL lepton selection. The $H_T > 300\,\text{GeV}$ requirement is applied in all search regions in this category.

N_b	M_T^{min} (GeV)	H_T (GeV)	$E_T^{miss} \in [50-200]\,\text{GeV}$	$E_T^{miss} > 200\,\text{GeV}$
0	< 120	> 300	SR1	SR2
1	< 120		SR3	SR4
2	< 120		SR5	SR6
3+	< 120		SR7	
inclusive	> 120		SR8	

threshold value. The use of p_T^{corr} reduces the difference of lepton kinematics between the measurement region and the application region. As nonprompt electrons are sensitive to the flavor of the originating parton, the loose electron selection is tuned in order to mitigate the flavor dependence with a relaxed identification criteria in addition to looser isolation selection.

Standard model processes producing prompt SS lepton pairs are estimated from simulation, except for the WZ background. Experimental and theoretical uncertainties are taken into account. The WZ background is taken from the simulation with a normalization taken from collision data in a dedicated control region. This region is defined by requiring three leptons with two of them forming a same-flavor opposite-sign pair with the invariant mass compatible with the Z boson mass, at least two jets, no b-tagged jets, and E_T^{miss} >30 GeV. The measured normalization factor is found to be 1.02 ± 0.27.

Background originating from misidentified charge is estimated from a control sample of events with opposite-sign lepton pairs, reweighted by the charge misidentification probability extracted from the simulation. For electrons, the probability is found to be O(10^{-5})–O(10^{-3}) depending on the electron p_T and η. The charged misidentification probability is scaled up by 20% after validating the method in a $Z \to ee$ control sample, where this scaling provides agreement between the estimate and observed misidentified charge background. Simulation studies find the charge misidentification probability for muons to be negligible.

5 Systematic uncertainties

Sources of systematic uncertainties affecting the normalization and relative population of signal and background processes are presented in this section and summarized in Table 6.

Experimental sources of uncertainty are related to the energy scales and identification efficiencies of objects used in the analysis. The jet energy scale (JES) uncertainty varies between 1 and 8%. The impact of this uncertainty is assessed by shifting the energy of each jet up or down by one standard deviation, before the computation of all kinematic observables. The variations are correlated among different signal regions, accounting for migration effects, and leading to uncertainties of 1–15%. Uncertainties associated to the jet b tagging efficiency are assigned in a similar way, leading to effects of order 1–15% for the $t\bar{t}W$ process.

Lepton identification and trigger efficiency are measured with the "tag-and-probe" technique [6, 7] with an uncertainty of 4–10% and 2–7%, respectively. The uncertainty in the modeling of pileup is 0–6%, while the integrated luminosity uncertainty is 6.2%.

Backgrounds estimated from simulation are subject to theoretical uncertainties in PDFs and in higher-order effects. The yield uncertainties related to PDFs are estimated by using the replica of the NNPDF 3.0 set, leading to a overall yield uncertainty of around 4% for the $t\bar{t}V$ ($V = W, Z$)

samples. The yield uncertainties related to higher-order effects are estimated by varying the renormalization and factorization scales up and down by a factor of two. The effect on the overall cross section is found to be 13% for $\mathrm{t\bar{t}W}$ and 11% for $\mathrm{t\bar{t}Z}$ for the NLO computation [23]. The effect on the acceptance is typically 5% for signal regions populated in events with less than 4 jets, and 10% for the LL signal regions. For regions with more hadronic energy, as the $\mathrm{t\bar{t}V}$ samples are generated at LO, extra shape uncertainties are considered to cover kinematic differences observed in the corresponding NLO samples: an extra uncertainty in the acceptance of 40% is considered for signal regions with at least five jets, and 100% for signal regions with $H_\mathrm{T} > 1125\,\mathrm{GeV}$. A similar procedure is used for the $\mathrm{W^{\pm}W^{\pm}}$ process leading to an overall uncertainty of 30%, while a 50% uncertainty is assigned to the other rare processes. Additional details can be found in Ref. [4].

Other sources of uncertainty are related to the estimation of the nonprompt lepton, WZ, and charge misidentification backgrounds from data. An overall normalization uncertainty of 30% is assigned to the nonprompt lepton background prediction, accounting for the performance of the method and the different application of the estimation methods described in Ref. [4]. An additional systematic uncertainty, between 1 and 50%, is associated to the subtraction of Drell–Yan and $\mathrm{W}+$jets events from the multijet control region. Statistical uncertainty in the number of events selected in the application regions is also considered.

A systematic uncertainty of 20% is assigned to the background yield from charge misidentification processes. This uncertainty corresponds to the correction derived in the $\mathrm{Z} \to \mathrm{e^{\pm}e^{\pm}}$ control sample in data. The estimation of the WZ background is assigned a 20% normalization uncertainty from the total uncertainty in the control region, combining a statistical component and a systematic uncertainty in the subtraction of the non-WZ processes in the control region. Using the same procedure as described above, uncertainties in the extrapolation from the control region to the signal region are assessed from the propagation of the uncertainty in the JES and in the b tagging efficiencies.

Table 6: Summary of the sources of uncertainties and their effect on the yield in the signal regions. Reported values are representative for the most relevant signal regions.

Source	Typical effect (%)
Integrated luminosity	6.2
Lepton selection	4–10%
Trigger efficiency	2–7
Pileup	0–6
Jet energy scale	1–15
b tagging	1–15
Monte Carlo stat.	1–100
Scale variations	10–100
PDFs	1-4
Nonprompt leptons	30–60
Charge misidentification	20
WZ normalization	20

6 Results

The distributions of the five kinematic variables used to define the signal regions (H_T, $E_\mathrm{T}^\mathrm{miss}$, $M_\mathrm{T}^\mathrm{min}$, N_jets, N_b) are shown in Fig. 2, after a preselection that requires SS lepton pair passing nominal selection criteria, at least two jets, and either $E_\mathrm{T}^\mathrm{miss}$ larger than 30 GeV or H_T larger

than 500 GeV. The full background estimation procedure is used. Event yields in the signal regions after full selection are presented in Fig. 3 and in Table 7; no significant deviation from the prediction is observed.

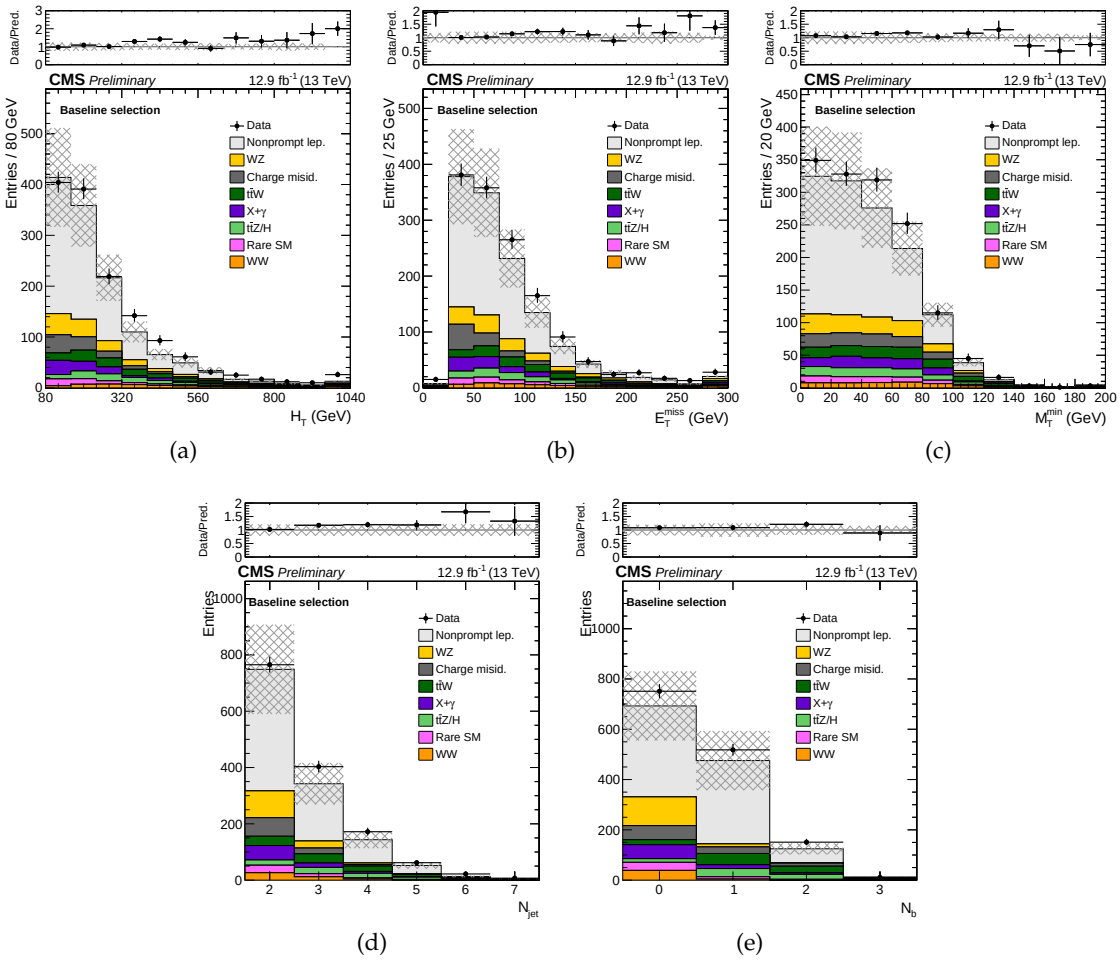

Figure 2: Distributions for the main analysis variables after the baseline selection with $\mathcal{L} = 12.9\,\text{fb}^{-1}$. The shaded area represents the total uncertainty in the background prediction.

No significant excess of events is observed over the SM expectations, and we use the results to constrain several simplified SUSY models as a function of the masses of the produced SUSY particle and the LSP. Results from all signal regions are combined to extract exclusion limits at 95% confidence level (CL), using the asymptotic formulation of the modified frequentist CL_s criterion [24–27]. Signal and background uncertainties described in Section 5 are included as nuisance parameters, taking into account correlation effects among different processes and signal regions when relevant.

The resulting limits on the cross section times branching fraction of SUSY particles, as well as the exclusion contours, are shown in Fig. 4 for the T1tttt model, and in Fig. 5 for two different assumptions for the chargino ($\tilde{\chi}^{\pm}$) mass in the T5qqqqWW model: $m_{\tilde{\chi}_1^{\pm}} = 0.5(m_{\tilde{\text{g}}} + m_{\tilde{\chi}^0})$ and $m_{\tilde{\chi}_1^{\pm}} = m_{\tilde{\chi}^0} + 20\,\text{GeV}$. The exclusion contours are obtained with the production cross section calculated at NLO+NLL (next-to-leading logarithmic) accuracy, assuming that all SUSY particles other than those included in the respective diagrams are heavy enough to be decoupled [28–34]. In general, the search regions with the largest sensitivity are HH SR30-33, requiring large E_T^miss or H_T. Depending on the model and the mass, other regions with softer kine-

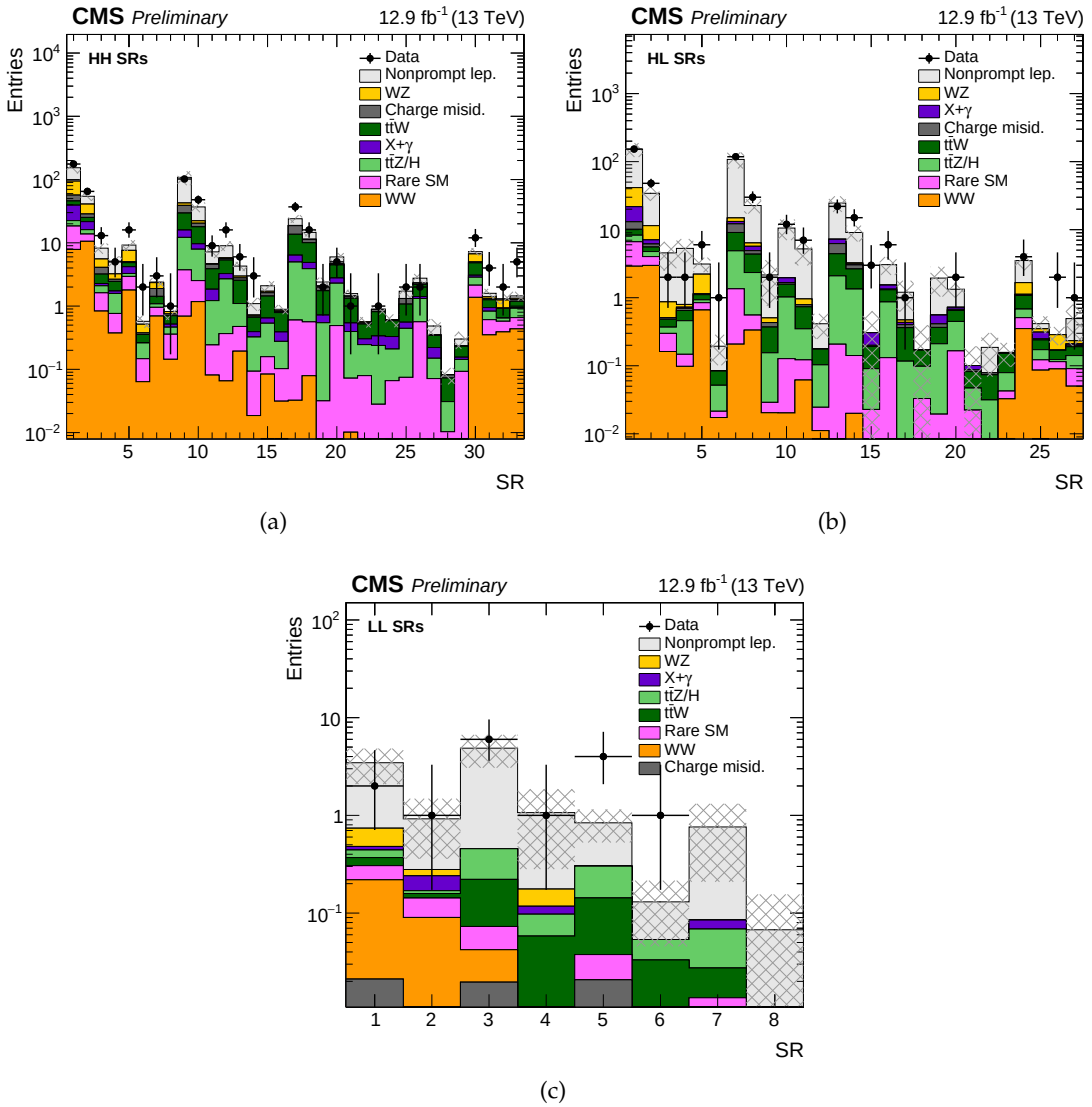

Figure 3: Event yields in HH (a), HL (b), and LL (c) signal regions with $\mathcal{L} = 12.9\,\text{fb}^{-1}$. The shaded area represents the total uncertainty in the background prediction.

Table 7: Event yields in the signal regions with $\mathcal{L} = 12.9\,\text{fb}^{-1}$.

	HH regions		HL regions		LL regions	
	Expected SM	Observed data	Expected SM	Observed data	Expected SM	Observed data
SR1	153.8 ± 29.2	176	151.8 ± 37.6	153	3.5 ± 1.5	2
SR2	54.4 ± 8.3	65	34.2 ± 8.1	48	0.92 ± 0.56	1
SR3	8.2 ± 1.7	13	4.6 ± 2.1	2	4.9 ± 1.8	6
SR4	5.1 ± 1.3	5	5.3 ± 2.0	2	1.07 ± 0.79	1
SR5	9.2 ± 1.7	16	3.13 ± 0.74	6	0.84 ± 0.35	4
SR6	0.57 ± 0.14	2	0.19 ± 0.10	1	0.13 ± 0.08	1
SR7	2.40 ± 0.36	3	107.8 ± 30.1	118	0.76 ± 0.55	0
SR8	0.82 ± 0.22	1	22.6 ± 5.6	30	0.07 ± 0.06	0
SR9	108.3 ± 26.1	102	2.2 ± 1.4	2		
SR10	36.9 ± 6.0	48	10.6 ± 3.6	12		
SR11	7.2 ± 1.5	9	5.2 ± 2.2	7		
SR12	9.0 ± 1.9	16	0.41 ± 0.17	0		
SR13	4.29 ± 0.70	6	24.6 ± 6.4	22		
SR14	1.09 ± 0.28	3	9.1 ± 2.4	15		
SR15	2.10 ± 0.39	0	0.31 ± 0.33	3		
SR16	0.89 ± 0.15	0	3.06 ± 0.97	6		
SR17	24.0 ± 3.2	37	1.20 ± 0.58	1		
SR18	14.6 ± 1.8	16	0.17 ± 0.23	0		
SR19	2.40 ± 0.39	2	1.94 ± 0.91	0		
SR20	6.0 ± 1.3	5	1.33 ± 0.32	2		
SR21	1.58 ± 0.21	1	0.10 ± 0.09	0		
SR22	0.56 ± 0.15	0	0.19 ± 0.13	0		
SR23	0.89 ± 0.14	1	0.16 ± 0.06	0		
SR24	0.60 ± 0.14	0	3.52 ± 0.98	4		
SR25	1.72 ± 0.35	2	0.42 ± 0.14	0		
SR26	2.76 ± 0.44	2	0.29 ± 0.08	2		
SR27	0.48 ± 0.15	0	0.49 ± 0.24	1		
SR28	0.08 ± 0.02	0				
SR29	0.30 ± 0.09	0				
SR30	7.26 ± 0.90	12				
SR31	1.59 ± 0.47	4				
SR32	1.31 ± 0.24	2				
SR33	1.45 ± 0.44	5				

matics contribute significantly to the sensitivity. In the regions of SUSY parameter space with a large mass difference between the gluino and the LSP, the results are rather stable with respect to the LSP mass variations, and gluino masses up to 1350 GeV are excluded in the T1tttt model, and up to 1100 GeV in the T5qqqqWW model with large mass splitting between the chargino and LSP. As the difference between the gluino and LSP masses becomes small, the acceptance decreases and the gluino mass limit becomes weaker, down to about 1100 GeV for an LSP mass of 850 GeV for the T1tttt model, and around 200 GeV lower for the T5qqqqWW model. The degradation of the limit with increasing LSP mass is much faster in the T5qqqqWW model with small mass splitting between chargino and LSP, as the W bosons are always produced off-shell and the lepton momenta depend strongly on the chargino boost.

In addition to the limits on simplified SUSY models, the results are also used to set 95% CL upper limits on the cross section for $\mathrm{t\bar{t}}\,\mathrm{t\bar{t}}$ production, as well as for SS top quark production. For $\mathrm{t\bar{t}}\,\mathrm{t\bar{t}}$ production, the cross section predicted by the SM at NLO precision [16] is 9.1 fb, and the upper limit on $\sigma(\mathrm{pp} \to \mathrm{tt\bar{t}\bar{t}})$ is found to be 57 fb, with an expected result of 46^{+23}_{-15} fb. For SS top quark pair production, the limit is obtained using events satisfying the baseline selection, categorized according to the number of b jets, and relying on the detector acceptance and selection efficiency of SM $\mathrm{t\bar{t}}$ events (apart from the charge requirement). The observed (expected) limit on $\sigma(\mathrm{pp} \to \mathrm{tt}) + \sigma(\mathrm{pp} \to \mathrm{\bar{t}\bar{t}})$ is 1.4 pb (0.9+/-0.4 pb). This limit should be considered approximate, as the kinematics of SS top quark pair production in general are different from those of $\mathrm{t\bar{t}}$ production, and the exact acceptance value depends on the details of the production mechanism.

Finally, we extract model independent limits on $\sigma \cdot \mathcal{A} \cdot \epsilon$, with σ the production cross section, $\mathcal{A}$ the kinematical and geometrical acceptance and ϵ the selection efficiency, in the two semi-inclusive regions with large $E_{\mathrm{T}}^{\mathrm{miss}}$ or large H_{T}. We combine HH SR30 and HH SR32 to compute the limit as a function of the minimum threshold on $E_{\mathrm{T}}^{\mathrm{miss}}$ (for $H_{\mathrm{T}} > 300$ GeV), and we similarly combine HH SR31 and HH SR33 to compute the limit as function of the H_{T} threshold (for $50 < E_{\mathrm{T}}^{\mathrm{miss}} < 300$ GeV). The limits are computed assuming full efficiency for $E_{\mathrm{T}}^{\mathrm{miss}}$ and H_{T}, while the lepton efficiency ranges 50–75% (70–90%) for generated electrons (muons) with $|\eta| < 2.4$ and $p_{\mathrm{T}} > 25$ GeV, increasing as a function of p_{T} and reaching the plateau value for $p_{\mathrm{T}} > 60$ GeV. The $\mathrm{CL_s}$ criterion without the asymptotic approximation is used. Results are shown in Fig. 6.

7 Summary

We have presented the results of a search for new physics in same-sign dilepton events using the CMS detector at the LHC, based on a proton-proton collision data sample at $\sqrt{s} = 13$ TeV corresponding to an integrated luminosity of 12.9 fb^{-1}, collected in the first half of 2016. The data are analyzed in exclusive signal regions defined with different selections on lepton and event kinematic variables, as well as jet and b jet multiplicities.

No significant deviations from the standard model expectations are observed. The results are used to set upper limits on the gluino pair production of supersymmetric particles in two simplified models. Gluino masses are probed up to 1350 GeV, extending the sensitivity of previous dilepton searches. In addition, 95% confidence level limits of 1.4 pb and 57 fb are set on the production cross section of two SS top quarks and $\mathrm{t\bar{t}}\,\mathrm{t\bar{t}}$, respectively, and model independent limits and selection efficiencies are provided to allow further interpretations of the results.

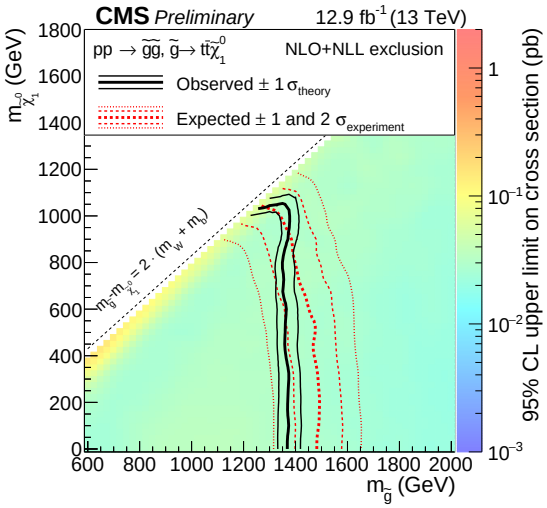

Figure 4: Exclusion regions at 95% CL in the plane of $m(\widetilde{\chi}^0)$ versus $m(\widetilde{g})$ for the T1tttt simplified model. The right-hand-side color scale indicates the excluded cross section values for a given point in the SUSY particle mass plane. Observed and expected limit lines indicate the boundaries of excluded regions (to the left and below the curve).

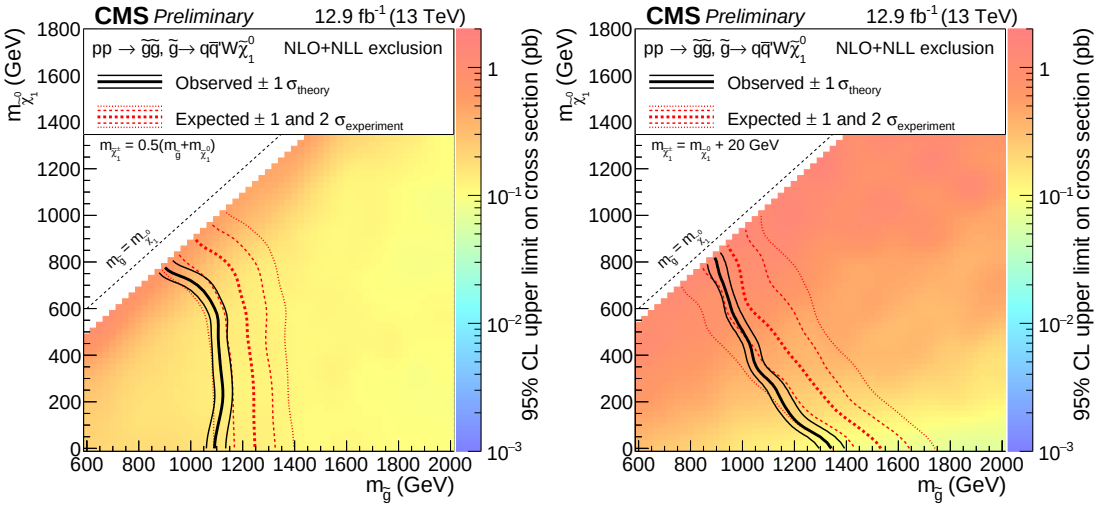

Figure 5: Exclusion regions at 95% CL in the plane of $m(\widetilde{\chi}^0)$ versus $m(\widetilde{g})$ for the T5qqqqWW simplified model with $m_{\widetilde{\chi}_1^\pm} = 0.5(m_{\widetilde{g}} + m_{\widetilde{\chi}^0})$ (left) and $m_{\widetilde{\chi}_1^\pm} = m_{\widetilde{\chi}^0} + 20\,\text{GeV}$ (right). The right-hand-side color scale indicates the excluded cross section values for a given point in the SUSY particle mass plane. Observed and expected limit lines indicate the boundaries of excluded regions (to the left and below the curve).

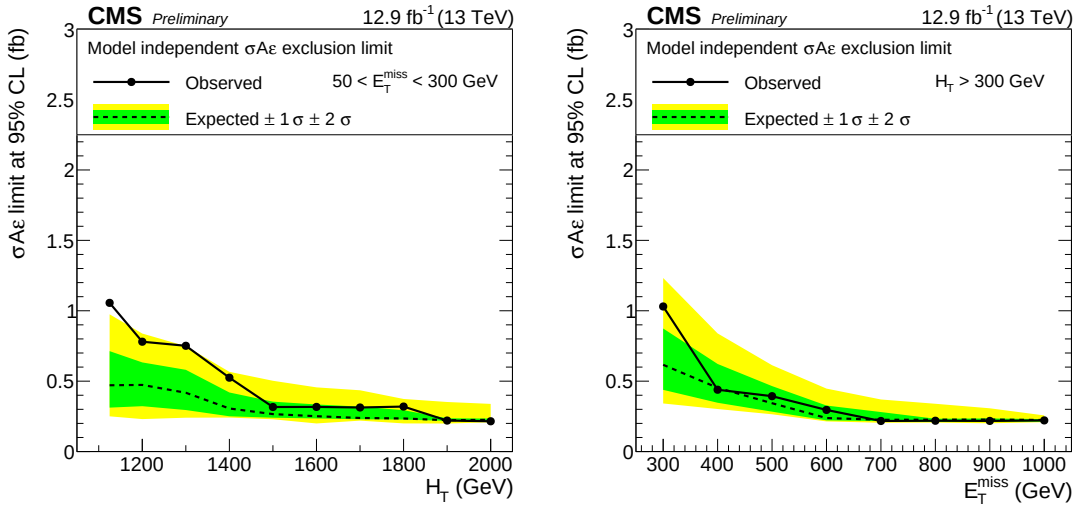

(a) (b)

Figure 6: Limits on $\sigma \cdot \mathcal{A} \cdot \epsilon$ at 95% CL.

References

[1] CMS Collaboration, "The CMS experiment at the CERN LHC", *JINST* **3** (2008) S08004, doi:10.1088/1748-0221/3/08/S08004.

[2] CMS Collaboration, "Search for new physics in events with same-sign dileptons and b jets in pp collisions at $\sqrt{s} = 8$ TeV", *JHEP* **03** (2013) 037, doi:10.1007/JHEP03(2013)037, 10.1007/JHEP07(2013)041, arXiv:1212.6194.

[3] CMS Collaboration, "Search for new physics in events with same-sign dileptons and jets in pp collisions at 8 TeV", *JHEP* **01** (2014) 163, doi:10.1007/JHEP01(2014)163, arXiv:1311.6736.

[4] CMS Collaboration, "Search for SUSY in same-sign dilepton events at 13 TeV", arXiv:1605.03171. *Accepted by Eur. Phys. J. C*.

[5] ATLAS Collaboration, "Search for supersymmetry at $\sqrt{s} = 13$ TeV in final states with jets and two same-sign leptons or three leptons with the ATLAS detector", *The European Physical Journal C* **76** (2016), no. 5, 1–26, doi:10.1140/epjc/s10052-016-4095-8.

[6] CMS Collaboration, "Performance of Electron Reconstruction and Selection with the CMS Detector in Proton-Proton Collisions at vs = 8 TeV", *JINST* **10** (2015) P06005, doi:10.1088/1748-0221/10/06/P06005, arXiv:1502.02701.

[7] CMS Collaboration, "Performance of CMS muon reconstruction in pp collision events at sqrt(s) = 7 TeV", *JINST* **7** (2012) P10002, doi:10.1088/1748-0221/7/10/P10002, arXiv:1206.4071.

[8] K. Rehermann and B. Tweedie, "Efficient Identification of Boosted Semileptonic Top Quarks at the LHC", *JHEP* **03** (2011) 059, doi:10.1007/JHEP03(2011)059, arXiv:1007.2221.

[9] CMS Collaboration, "Particle-flow event reconstruction in CMS and performance for jets, taus, and $E_{\mathrm{T}}^{\mathrm{miss}}$", CMS Physics Analysis Summary CMS-PAS-PFT-09-001, CERN, 2009.

[10] CMS Collaboration, "Commissioning of the particle-flow event reconstruction with the first LHC collisions recorded in the CMS detector", CMS Physics Analysis Summary CMS-PAS-PFT-10-001, CERN, 2010.

[11] M. Cacciari, G. P. Salam, and G. Soyez, "The anti-k_{T} jet clustering algorithm", *JHEP* **04** (2008) 063, doi:10.1088/1126-6708/2008/04/063, arXiv:0802.1189.

[12] CMS Collaboration, "Jet Energy Calibration in the 8 TeV pp data", CMS Physics Analysis Summary CMS-PAS-JME-13-004, 2015.

[13] CMS Collaboration, "Identification of b-quark jets with the CMS experiment", *JINST* **8** (2013) P04013, doi:10.1088/1748-0221/8/04/P04013, arXiv:1211.4462.

[14] CMS Collaboration, "Performance of b tagging at $\sqrt{s} = 8$ TeV in multijet, $\mathrm{t\bar{t}}$ and boosted topology events", CMS Physics Analysis Summary CMS-PAS-BTV-13-001, 2013.

[15] CMS Collaboration, "Identification of double-b quark jets in boosted event topologies", CMS Physics Analysis Summary CMS-PAS-BTV-15-002, 2016.

[16] J. Alwall et al., "The automated computation of tree-level and next-to-leading order differential cross sections, and their matching to parton shower simulations", *JHEP* **07** (2014) 079, doi:10.1007/JHEP07(2014)079, arXiv:1405.0301.

[17] T. Melia, P. Nason, R. Rontsch, and G. Zanderighi, "W^+W-, WZ and ZZ production in the POWHEG BOX", *JHEP* **11** (2011) 078, doi:10.1007/JHEP11(2011)078, arXiv:1107.5051.

[18] T. Sjostrand, S. Mrenna, and P. Z. Skands, "A Brief Introduction to PYTHIA 8.1", *Comput. Phys. Commun.* **178** (2008) 852, doi:10.1016/j.cpc.2008.01.036, arXiv:0710.3820.

[19] CMS Collaboration, "Event generator tunes obtained from underlying event and multiparton scattering measurements", *Eur. Phys. J. C* **76** (2016) 155, doi:10.1140/epjc/s10052-016-3988-x, arXiv:1512.00815.

[20] GEANT4 Collaboration, "GEANT4—a simulation toolkit", *Nucl. Instrum. Meth. A* **506** (2003) 250, doi:10.1016/S0168-9002(03)01368-8.

[21] S. Abdullin et al., "The fast simulation of the CMS detector at LHC", *J. Phys. Conf. Ser.* **331** (2011) 032049, doi:10.1088/1742-6596/331/3/032049.

[22] N. Collaboration, "Parton distributions for the LHC Run II", *JHEP* **04** (2015) 040, doi:doi:10.1007/JHEP04(2015)040, arXiv:1410.8849.

[23] M. V. Garzelli, A. Kardos, C. G. Papadopoulos, and Z. Trocsanyi, "$t\bar{t}W^{\pm}$ and $t\bar{t}Z$ Hadroproduction at NLO accuracy in QCD with Parton Shower and Hadronization effects", *JHEP* **11** (2012) 056, doi:10.1007/JHEP11(2012)056, arXiv:1208.2665.

[24] G. Cowan, K. Cranmer, E. Gross, and O. Vitells, "Asymptotic formulae for likelihood-based tests of new physics", *Eur. Phys. J. C* **71** (2011) 1554, doi:10.1140/epjc/s10052-011-1554-0, arXiv:1007.1727. [Erratum: doi:10.1140/epjc/s10052-013-2501-z].

[25] A. L. Read, "Presentation of search results: The CL_S technique", *J. Phys. G* **28** (2002) 2693, doi:10.1088/0954-3899/28/10/313.

[26] T. Junk, "Confidence level computation for combining searches with small statistics", *Nucl. Instrum. Meth. A* **434** (1999) 435, doi:10.1016/S0168-9002(99)00498-2, arXiv:hep-ex/9902006.

[27] ATLAS and CMS Collaborations, "Procedure for the LHC Higgs boson search combination in summer 2011", ATL-PHYS-PUB-2011-011, CMS NOTE-2011/005, 2011.

[28] W. Beenakker, R. Höpker, M. Spira, and P. M. Zerwas, "Squark and gluino production at hadron colliders", *Nucl. Phys. B* **492** (1997) 51, doi:10.1016/S0550-3213(97)80027-2, arXiv:hep-ph/9610490.

[29] A. Kulesza and L. Motyka, "Threshold resummation for squark-antisquark and gluino-pair production at the LHC", *Phys. Rev. Lett.* **102** (2009) 111802, doi:10.1103/PhysRevLett.102.111802, arXiv:0807.2405.

[30] A. Kulesza and L. Motyka, "Soft gluon resummation for the production of gluino-gluino and squark-antisquark pairs at the LHC", *Phys. Rev. D* **80** (2009) 095004, doi:10.1103/PhysRevD.80.095004, arXiv:0905.4749.

[31] W. Beenakker et al., "Soft-gluon resummation for squark and gluino hadroproduction", *JHEP* **12** (2009) 041, doi:10.1088/1126-6708/2009/12/041, arXiv:0909.4418.

[32] W. Beenakker et al., "Squark and gluino hadroproduction", *Int. J. Mod. Phys. A* **26** (2011) 2637, doi:10.1142/S0217751X11053560, arXiv:1105.1110.

[33] M. Krämer et al., "Supersymmetry production cross sections in pp collisions at $\sqrt{s} = 7$ TeV", (2012). arXiv:1206.2892.

[34] C. Borschensky et al., "Squark and gluino production cross sections in pp collisions at $\sqrt{s}$ = 13, 14, 33 and 100 TeV", *Eur. Phys. J. C* **74** (2014) 3174, doi:10.1140/epjc/s10052-014-3174-y, arXiv:1407.5066.